lubricants

Article

Reynolds Model versus JFO Theory in Steadily Loaded Journal Bearings

Wanjun Xu [1,*], Shanhui Zhao [1], Yaoyao Xu [1] and Kang Li [2]

[1] School of Energy and Power Engineering, Nanjing Institute of Technology, Nanjing 211167, China; shhzhaoseu@163.com (S.Z.); x00207180145@njit.edu.cn (Y.X.)
[2] School of Energy, Power and Mechanical Engineering, North China Electric Power University, Baoding 071003, China; kangli@ncepu.edu.cn
* Correspondence: j00000003084@njit.edu.cn

Abstract: Cavitation has a potential effect on the performance of full circle journal bearings. This paper studied the effects of cavitation on steadily loaded journal bearings, with the purpose of analyzing the necessity of adopting a mass-conserving model for ordinary journal bearings. The Christopherson's method and Elrod cavitation algorithm were implemented to represent the non-mass-conserving Reynolds model and the mass-conserving Jakobsson-Floberg-Olsson (JFO) theory, respectively. The difference in the oil film reformation boundaries predicted by the two methods was focused on. The typical performance parameters including oil film pressure, load-carrying capacity, attitude angle, friction force, and leakage were comprehensively compared. The results show that the load-carrying capacity is improved by the decrease in cavitation pressure, and the effect is significant in lightly loaded cavitated bearings. In non-cavitated cases and the cavitated cases with intermediate and heavy loads, the difference between the Reynolds model and the JFO theory can be effectively ignored, but the accuracy of the leakage predicted using the Reynolds model should be carefully evaluated.

Keywords: cavitation; JFO theory; Elrod algorithm; Reynolds boundary condition; journal bearing

Citation: Xu, W.; Zhao, S.; Xu, Y.; Li, K. Reynolds Model versus JFO Theory in Steadily Loaded Journal Bearings. *Lubricants* **2021**, *9*, 111. https://doi.org/10.3390/lubricants9110111

Received: 18 October 2021
Accepted: 16 November 2021
Published: 19 November 2021

1. Introduction

Cavitation is a complex phenomenon that usually occurs in the region where the liquid pressure is below cavitation pressure [1,2]. When it occurs, gas will escape (or vaporize) from the liquid, forms bubbles, and occupy part of the space. The bubbles result in a change of pressure and make the bearing behave differently. Generally, cavitation is divided into air cavitation and vapor cavitation [3]. Air cavitation is air dissolved in oil escaping from the solution. It occurs when the pressure is below saturation pressure. Vapor cavitation is due to the pressure being lower than the saturated vapor pressure, where the oil boils to form bubbles [4]. No matter what kind of cavitation, they represent the rupture and reformation of the oil film. In full circle journal bearings with stationary load, cavitation takes place in the section of divergent clearance region. The oil film is separated by finger-shaped voids (cavities), and the shape of the cavitated region remains relatively stable.

Two methods, namely the Reynolds model [5] and the Jakobsson–Floberg–Olsson (JFO) theory [6,7], are commonly used to evaluate the bearing performance. The well-known Reynolds boundary condition belongs to the Reynolds model. It requires the pressure derivative smoothly approaching zero to locate the oil film rupture boundary. The oil film reformation boundary is not explained in the Reynolds boundary condition. However, in the numerical solution of the Reynolds equation, an algorithm that sets the negative pressure to zero, developed by Christopherson [8], provided an opportunity to locate the oil film reformation boundary. A complete shape of the cavitated region can be obtained by choosing a cavitation pressure lower than 0 Pa (ambient pressure).

The oil film reformation boundary is curious because it is an additional product within Christopherson's method. The effect of the oil film reformation boundary on the Reynolds model's accuracy is unclear. In practical calculations, the cavitation pressures of 0 Pa and lower than 0 Pa are both applied [9–12]. The Reynolds model with a cavitation pressure lower than 0 Pa has not been fully studied.

The JFO theory is an improvement to the Reynolds model due to density term being preserved in the mass continuity equation. It incorporates the Reynolds boundary condition and provides the oil film reformation boundary condition. A detailed explanation of the oil film reformation boundary condition can be seen in [6,7]. The JFO theory is well accepted because it obeys the law of conservation of mass, and had been validated by experiments [6,7]. A variety of algorithms [10,13–17] have been developed for implementing the JFO theory, such as the well-known Elrod algorithm [13]. Although the complexity of the algorithm is higher than the Christopherson's method, it was largely used in studying cavitation and its effect on bearing characteristics [18,19].

The effects of cavitation on the journal bearing characteristics are mainly reflected in load capacity, friction force, leakage, etc. The effect of load capacity is generally considered not to be significant, because cavitation always occurs out of the positive pressure region [20]. The friction force is significantly affected by the cavitation, as almost half of the region is dominated by the cavitation, where the friction characteristic is changed by the separation of oil and gas [10]. The accuracy of the predicted leakage depends on the location of the oil film reformation boundary. It is a primary sign reflecting the difference between the Reynolds model and the JFO theory.

Moreover, cavitation plays a key role in surface textured bearings [1,21]. The bearing performance is altered by adding surface texture (such as dimples). Cavitation will occur in local divergent gaps and thus alters the established hydrodynamic pressure. A lot of research has been devoted to this area [22–28]. Promising results have been obtained [21,29–32], although a consistent conclusion has not been reached. Cavitation behavior is complex in surface textures due to the variation of cavitation pressure, rotational speed, pattern/distribution of textures, etc. The adoption of a mass-conserving model has been widely recognized for analyzing surface textured bearings [10].

Although the effect of cavitation has been investigated for ordinary journal bearings [1–4], the presentation of results is still insufficient. The evaluation of the difference between a non-mass-conserving model and a mass-conserving model is not clear. In this paper, a comprehensive analysis was conducted to study the effects of cavitation on the performance of steadily loaded journal bearings. The Christopherson's method and Elrod cavitation algorithm were implemented to represent the Reynolds model and the JFO theory, respectively. The two methods were compared under different cavitation pressures. The typical performance parameters including oil film pressure, load-carrying capacity, attitude angle, friction force, and leakage were analyzed. The aim of the paper is twofold: (1) The effect of cavitation on bearing characteristics is presented. The results are beneficial for the understanding of lightly loaded cavitated bearings due to the amplified cavitation effect. (2) The comparison of the Reynolds model and the JFO theory was investigated. The purpose was to analyze the necessity of adopting a mass-conserving model for ordinary journal bearings. The accuracy of the Reynolds model was analyzed by focusing on the location of the inaccurate oil film reformation boundary. It helps to understand the non-mass-conserving Reynolds model.

2. Theoretical Model

2.1. Reynolds Model

For a Newtonian lubricant with constant viscosity, the incompressible Reynolds equation is expressed as follows:

$$\frac{\partial}{\partial x}\left(h^3\frac{\partial p}{\partial x}\right)+\frac{\partial}{\partial y}\left(h^3\frac{\partial p}{\partial y}\right)=6\mu U\frac{\partial h}{\partial x} \tag{1}$$

where h is the film thickness, p is the pressure, μ is the dynamic viscosity, and U is the sliding speed. The pressure is governed by the Reynolds equation throughout the whole bearing clearance region. Equation (1) was numerically solved using the finite difference method. The process is ignored since the solution method is well known. Here, it is noted that the Christopherson's method was embedded in the loop by using an if-else-end statement. That is, if the nodal pressure is lower than the predetermined cavitation pressure, the nodal pressure is assigned as the cavitation pressure. Using the Christopherson's method, the rupture and reformation boundaries were both obtained. The results of the Reynolds model were compared with the results of the JFO theory.

2.2. JFO Theory

Equation (1) is transformed into the compressible Reynolds equation by preserving the density term, as follows:

$$\frac{\partial}{\partial x}\left(\rho h^3 \frac{\partial p}{\partial x}\right) + \frac{\partial}{\partial y}\left(\rho h^3 \frac{\partial p}{\partial y}\right) = 6\mu U \frac{\partial(\rho h)}{\partial x} \tag{2}$$

where ρ is the density. By the idea of a universal partial differential equation (PDE) [13], Equation (2) is changed to

$$\frac{\beta}{12\mu}\frac{\partial}{\partial x}\left(\frac{gh^3\partial\theta}{\partial x}\right) + \frac{\beta}{12\mu}\frac{\partial}{\partial y}\left(\frac{gh^3\partial\theta}{\partial y}\right) = \frac{U}{2}\frac{\partial(h\theta)}{\partial x} \tag{3}$$

where β is the lubricant bulk modulus, g is the switch function, and θ is the density ratio of ρ/ρ_c. The value of θ can be regarded as a fractional film content or the oil film height through the striations [10]. The pressure–density relation is

$$p = p_c + \beta \ln \theta \tag{4}$$

where p_c is the cavitation pressure. The definition of g suggested by Elrod [13] is expressed as

$$g = \begin{cases} 1 & \theta \geq 1 \\ 0 & \theta < 1 \end{cases} \tag{5}$$

Equation (3) is an elliptic PDE in the liquid region (g = 1) and a hyperbolic PDE in the cavitated region (g = 0). Different discrete schemes are required. The complete discrete schemes were provided in [14]. It is noted that the switch function $g(x,y)$ was employed not only to remove the pressure terms in the cavitated region but also to revise the discrete scheme of the shear flow term. The modified switch function algorithm developed by Fesanghary and Khonsari [33] was employed to enhance the stability of the algorithm. The successive over relaxation method (SOR) was used to accelerate convergence. The solution method is the same to that of the Reynolds model. The flow chart for the procedure is shown in Figure 1.

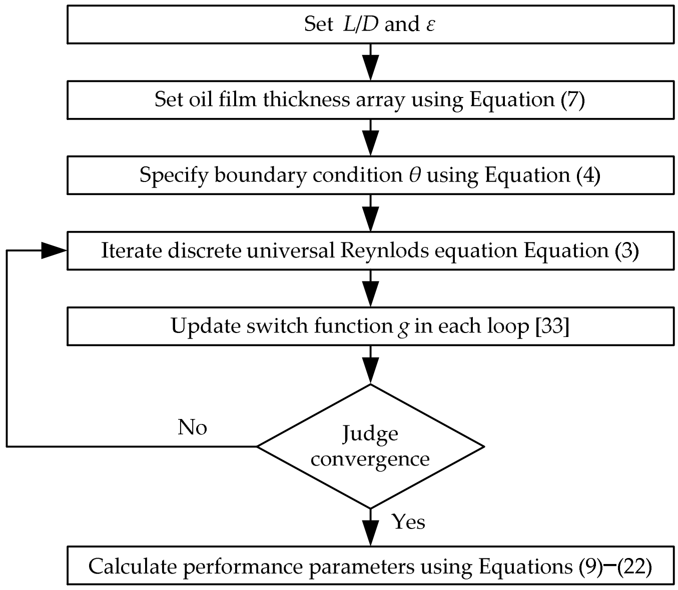

Figure 1. The flow chart of the procedure.

Owing to the complexity of the Elrod algorithm, the obtained results were compared with the experimental results [6,7,34,35] for validation. The resulting central pressure for the journal bearing is shown in Figure 2. The predicted pressure shows a good agreement with the experimental result, and the accuracy is not very dependent on the number of grids. The mesh with 50 × 120 nodes (axial × circumferential) was adopted for the following calculations.

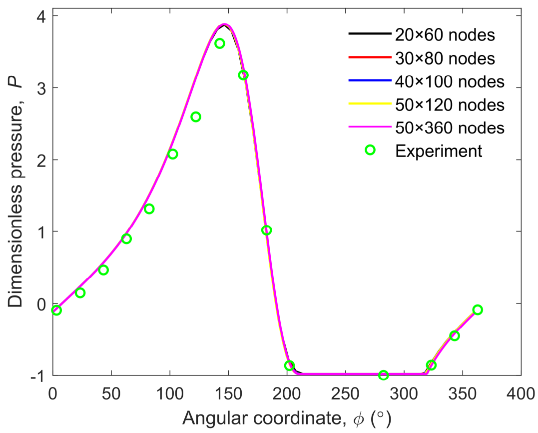

Figure 2. Central pressure variation for the journal bearing. (D = 100 mm, L = 133 mm, C/R = 0.00291, ε = 0.60, n = 459.3 r/min, μ = 0.0127 Pa·s, $p_c = -72.1$ kPa, $\beta = 1 \times 10^{10}$ Pa, $P = (p - p_a)\,(C/R)^2/(\mu\omega)$).

3. Bearing Condition and Parameters

The incompressible Reynolds equation is linear. When cavitation is considered, the preserved density term makes the Reynolds equation be nonlinear [36]. Hence, bearing number Λ is introduced to help analysis, as expressed by

$$\Lambda = \frac{6\mu\omega}{p_a}\left(\frac{R}{C}\right)^2 \tag{6}$$

where ω is the angular velocity, p_a is the ambient pressure, R is the journal radius, and C is the radius clearance.

A typical plain journal bearing was analyzed to present the effect of cavitation on the bearing characteristics and the difference to the Reynolds model. For the sake of simplicity, the bearing is considered unwrapped by ignoring the curvature, allowing for the use of Cartesian coordinate system. Consider a rectangle geometry that represents the bearing clearance region, as shown in Figure 3. Assuming the hydrodynamic film begins at h_{max}, the film thickness profile is expressed by

$$h = (1 + \varepsilon \cos \varphi)C \tag{7}$$

where ε is the eccentricity ratio and ϕ is the angle coordinate starting from h_{max}. Due to the use of the Cartesian coordinate system, the relation between ϕ and x is

$$x = \phi R \tag{8}$$

where $x = 0$, $\phi = 0$ is at the maximum film thickness, and $x = \pi R$, $\phi = \pi$ is at the minimum film thickness.

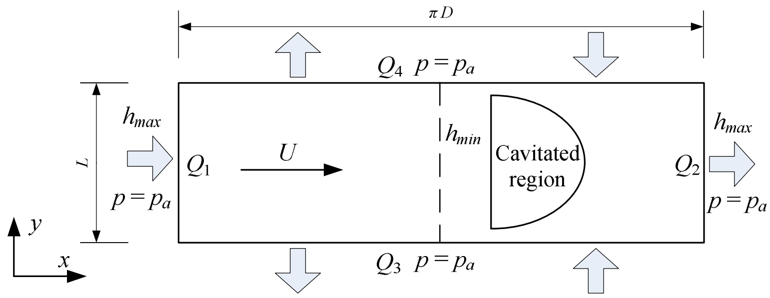

Figure 3. Plain journal bearings with oil supply at h_{max}.

Various methods are available for distributing lubricant for a journal bearing. Although different oil supply methods impact on the bearing characteristics differently, only a typical oil supply is considered here. The oil supply is kept along the axial clearance of h_{max}. In practical bearings, the position of h_{max} depends on the attitude angle that varies with load. The precise oil supply location is hard to maintain. However, this oil supply method was largely applied in theoretical analysis [3,36,37] because it presents the characteristics of a plane oil film. There are four boundaries around the bearing geometry. All of them are treated as the pressure boundary condition with $p_a = 0$ Pa. The bearing is considered as a submerged bearing.

The bearing performance parameters including oil film pressure p, load-carrying capacity W, attitude angle ψ, friction force F, and leakage q were analyzed below. For comparison purposes, all the performance parameters are taken as dimensionless forms. These performance parameters are calculated as follows. The dimensionless pressure $\overline{P}$ is defined by

$$\overline{P} = \frac{p - p_a}{\mu N_s}\left(\frac{C}{R}\right)^2 \tag{9}$$

where N_s is the rotational speed in rev/s. The radial and tangential loads, W_r and W_t, are, respectively calculated by

$$W_r = \int_0^{\pi D}\int_0^{L} p \cos \varphi R \mathrm{d}\varphi \mathrm{d}y \tag{10a}$$

$$W_t = \int_0^{\pi D}\int_0^{L} p \sin \varphi R \mathrm{d}\varphi \mathrm{d}y \tag{10b}$$

where D is the bearing diameter and L is the bearing length. The differential of $\mathrm{d}\phi$ satisfies $R\mathrm{d}\phi = \mathrm{d}x$. The attitude angle ψ is expressed by

$$\psi = \tan^{-1}(|W_t/W_r|) \tag{11}$$

The total load W is calculated by

$$W = \sqrt{W_r^2 + W_t^2} \tag{12}$$

The dimensionless load $\overline{W}$ is defined by

$$\overline{W} = \frac{W}{\pi \mu N_s DL}\left(\frac{C}{R}\right)^2 = \frac{1}{\pi S} \tag{13}$$

where S is the Sommerfeld number. The Sommerfeld number is written as

$$S = \frac{\mu N_s DL}{W}\left(\frac{R}{C}\right)^2 \tag{14}$$

The friction coefficient $(R/C)f$ is calculated by

$$\frac{R}{C}f = \frac{R}{C}\frac{F}{W} = \frac{R}{C}\frac{1}{W}\int_0^{\pi D}\int_0^{L}\left(\frac{\mu U}{h} + \frac{h}{2}\frac{\partial p}{\partial x}\right)\mathrm{d}x\mathrm{d}y \tag{15}$$

The friction coefficient calculated by Equation (15) is used to predict both the liquid and cavitated region, although it needs be more discussed due to the complex liquid–air separation. The dimensionless leakage $Q_{1,2,3,4}$ is given by

$$Q_1 = \frac{q_1}{\pi N_s RLC} = \frac{1}{\pi N_s RLC}\int_0^{L}\left(\frac{Uh}{2} - \frac{h^3}{12\mu}\frac{\partial p}{\partial x}\right)\bigg|_{x=0}\mathrm{d}y \tag{16}$$

$$Q_2 = \frac{q_2}{\pi N_s RLC} = \frac{1}{\pi N_s RLC}\int_0^{L}\left(\frac{Uh}{2} - \frac{h^3}{12\mu}\frac{\partial p}{\partial x}\right)\bigg|_{x=\pi D}\mathrm{d}y \tag{17}$$

$$Q_3 = \frac{q_3}{\pi N_s RLC} = \frac{1}{\pi N_s RLC}\int_0^{\pi D}\left(-\frac{h^3}{12\mu}\frac{\partial p}{\partial y}\right)\bigg|_{y=0}\mathrm{d}x \tag{18}$$

$$Q_4 = \frac{q_4}{\pi N_s RLC} = \frac{1}{\pi N_s RLC}\int_0^{\pi D}\left(-\frac{h^3}{12\mu}\frac{\partial p}{\partial y}\right)\bigg|_{y=L}\mathrm{d}x \tag{19}$$

Equations (16)–(19) are valid under the condition of full film boundary conditions ($\theta \geq 1$, submerged bearing).

4. Cavitation Analysis

Cavitation pressure is usually between ambient pressure and absolute zero pressure. Traditional bearing analysis often adopted 0 Pa as the cavitation pressure. This assumption is particularly suitable for the Reynolds model because oil film reformation cannot arise under the condition of cavitation pressure equaling oil supply pressure. Many works, as represented by Khonsari and Booser [3], have summarized the numerical solutions of plain journal bearings based on this assumption. In the JFO theory, the cavitation pressure can be taken as negative pressure, which is closer to the actual situation. The actual cavitation pressure varies with different bearings and operation conditions [4]. In the below analysis, the cavitation pressures of 0 Pa, -0.5×10^5 Pa and -1.0×10^5 Pa were analyzed for the two methods.

Figure 4 shows the central pressure variation with different p_c for the Reynolds model and the JFO theory. The pressure obtained using the Reynolds model is the same to that obtained using the JFO theory at the condition of cavitation pressure equaling ambient pressure (the black dotted line is covered by the black solid line). If the cavitation pressure is lower than the ambient pressure, the two methods provide different results. The oil film rupture boundary predicted using the Reynolds model is the same to that predicted using the JFO theory, but the oil film reformation boundary predicted using the Reynolds model is ahead of that predicted using the JFO theory. It implies that, the cavitated area is underestimated using the Reynolds model, and the difference between the two methods increases with the reducing cavitation pressure.

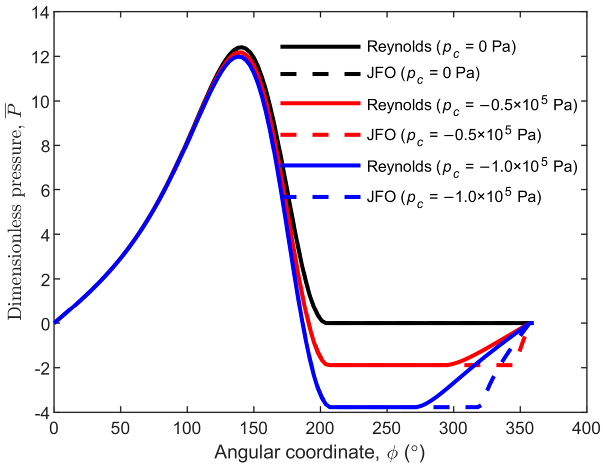

Figure 4. Central pressure variation with different p_c for Reynolds model and JFO theory at the condition of $L/D = 1$, $\varepsilon = 0.5$, and $\Lambda = 10$.

To further explain the difference, Figure 5a compares the pressure contours at $p_c = -0.5 \times 10^5$ Pa for the Reynolds model and the JFO theory. The pressure distribution in the liquid region is basically the same for the two methods, while the pressure distribution in the cavitated region is obviously different. The difference is mainly reflected by the different shapes of cavitated areas, as shown in Figure 5b. The cavitation patterns predicted using the two methods look like half ellipses. The major axis of the ellipse predicted using the Reynolds model is shorter than that predicted using the JFO theory. This difference is due to the fact that the density effect in the cavitated region is not reflected in the Reynolds model. In other words, mass conservation is not always satisfied with the Reynolds model. The quantitative effect of cavitation pressure on the bearing characteristics is presented below.

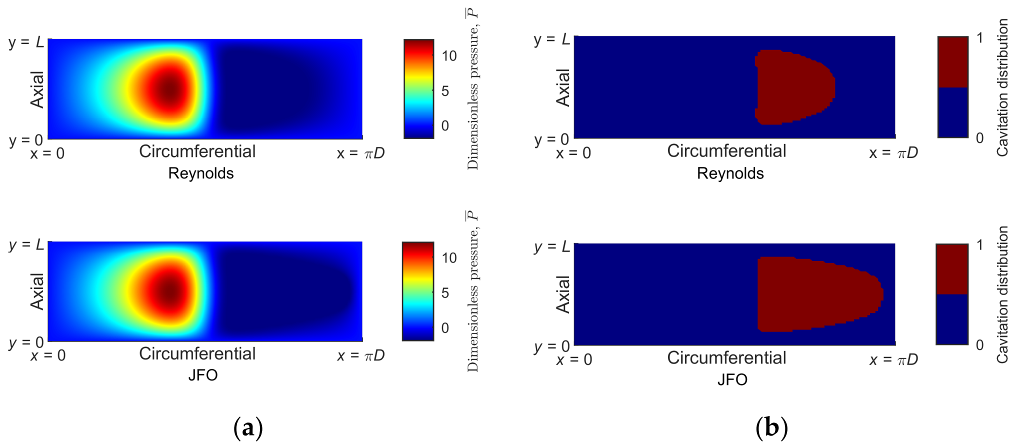

Figure 5. Pressure and cavitation distribution for $p_c = -0.5 \times 10^5$ Pa at the condition of $L/D = 1$, $\varepsilon = 0.5$, and $\Lambda = 10$: (**a**) Pressure distribution; (**b**) Cavitation distribution.

Figure 6 shows the effect of cavitation pressure on the Sommerfeld number for the Reynolds model and the JFO theory. The effects of the length to diameter ratio L/D, and eccentricity ratio ε are also presented. The Sommerfeld number S is an important parameter used to predict bearing characteristics. It represents the reciprocal load-carrying capacity, as related by $\overline{W} = 1/(\pi S)$. First of all, let us focus on the bearing with $p_c = 0$ Pa, as represented by the black lines. The resulting Sommerfeld number agrees well with the result provided by Khonsari and Booser [3] under different L/D and ε. Moreover, the Sommerfeld number predicted using the JFO theory is the same as that predicted using the Reynolds model (the black dotted lines are covered by the black solid lines), since there is no film reformation. Secondly, let us observe the blue lines that represent the bearings with $p_c = -1.0 \times 10^5$ Pa. (1) The Sommerfeld number of the bearing with $p_c = -1.0 \times 10^5$ Pa is smaller than that of the bearing with $p_c = 0$ Pa for most cases. It implies that the load-carrying capacity is enhanced by the reducing cavitation pressure, which is in accordance with the comment on cavitation by Dowson and Taylor [20]. (2) The difference in the Sommerfeld number between the different cavitation pressures gradually decreases with the increasing ε and L/D. This can be explained by the extent of the hydrodynamic effect. With the increase in ε and L/D, the convergence clearance becomes narrower, and more oil is kept in the clearance; hence, the hydrodynamic effect is enhanced. The positive pressure in the convergence clearance region is increased, while the negative pressure in the cavitated region is kept in the constant cavitation pressure. This behavior weakens the cavitation effect on the load-carrying capacity. (3) The Sommerfeld number predicted using the JFO theory is basically the same to that predicted using the Reynolds model for most cases. The slight difference appears in the condition of medium ε and large L/D, where the Sommerfeld number predicted using the JFO theory is slightly smaller than that predicted using the Reynolds model. It implies that the Reynolds model underestimates the load-carrying capacity. This is contrarily compared to the case of microtextured thrust bearings, in which the load-carrying capacity is overestimated using the Reynolds model. In journal bearings, the cavitated area can increase the load because the integral calculation is along the circular surface and the cavitated region is on the opposite side of the positive pressure region. Finally, the bearing with $p_c = -0.5 \times 10^5$ Pa is presented by the red lines. The variation behavior of the Sommerfeld number is between the two situations mentioned above.

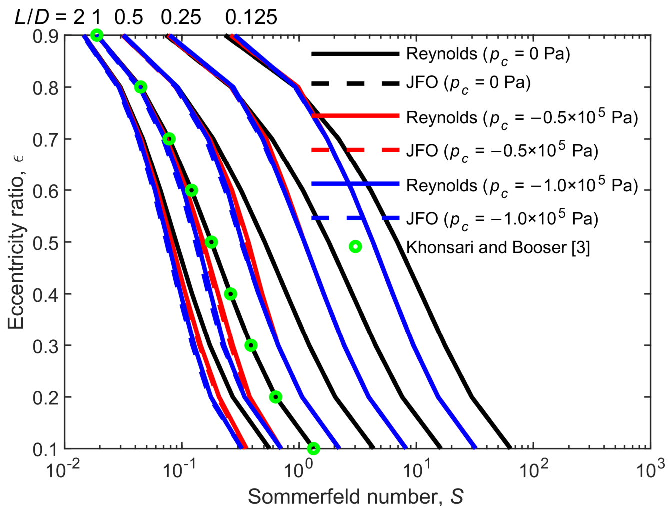

Figure 6. Effect of cavitation pressure on Sommerfeld number for Reynolds model and JFO theory at $\Lambda = 10$.

Figure 7 shows the effect of cavitation pressure on the attitude angle for the Reynolds model and the JFO theory. On the one hand, the resulting attitude angles predicted by the two methods are the same at the condition of $p_c = 0$ Pa for different L/D and ε (the black dotted lines are covered by the black solid lines), and agree well with the results provided by Khonsari and Booser [3]. On the other hand, (1) the effect of cavitation pressure on the attitude angle is larger than that on the Sommerfeld number. The attitude angle increases with the reducing cavitation pressure. This is due to the increase in the load-carrying capacity, making the bearing self-adjust to a large attitude angle to reduce the load. Moreover, the difference in the attitude angle between different cavitation pressures increases with the decrease in L/D. In extreme cases, the attitude angle reaches the maximum of 90°, which appears at the bearing with a small L/D and ε. In fact, the attitude angle of 90° is the full Sommerfeld solution. This is due to the weak hydrodynamic effect that cannot make cavitation occur. In other words, the negative pressure peak is higher than the predetermined cavitation pressure. (2) The attitude angle predicted using the Reynolds model is basically the same to that predicted using the JFO theory. This difference is not obvious.

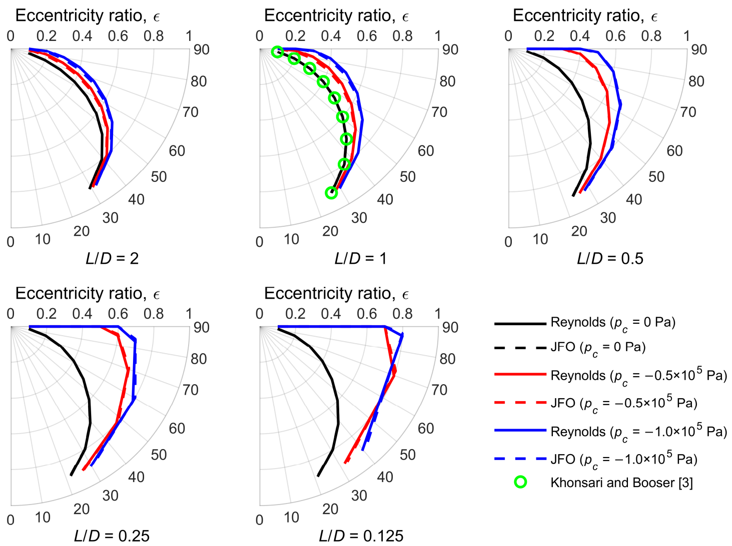

Figure 7. Effect of cavitation pressure on attitude angle for Reynolds model and JFO theory at $\Lambda = 10$.

Figure 8 shows the effect of cavitation pressure on the friction coefficient for the Reynolds model and the JFO theory. The friction coefficient $(R/C)f$ represents the ratio of friction force f to load capacity W. The variation of the friction coefficient is very similar to that of the Sommerfeld number. This is due to the characteristic of Petroff's formula, which indicates the relation between torque and power loss in a journal bearing [3]. In concentric bearing with zero eccentricity, the Petroff's formula reveals that the friction coefficient and the Sommerfeld number are related by

$$\frac{R}{C}f = 2\pi^2 S \tag{20}$$

where $2\pi^2$ indicates the Petroff multiplier [37]. The Petroff multiplier increases with the increasing eccentricity ratio. Hence, as the eccentricity ratio increases, the rate of decrease in the friction coefficient is slightly slower than that of the Sommerfeld number. Similar to the variation of the Sommerfeld number, the same behavior for the friction coefficient is obtained as (1) the friction coefficient decreases with the decreasing cavitation pressure for most cases; (2) the difference in the friction coefficient between different cavitation pressures gradually decreases with the increasing ε and L/D, since the hydrodynamic effect enhances; and (3) the friction coefficient is overestimated by the Reynolds model but the difference is small. In addition, the resulting friction coefficient is calculated by Equation (15), where the effect of θ on the friction coefficient is not considered. The viscous shear stress variation due to the cavitation effect needs to be further investigated.

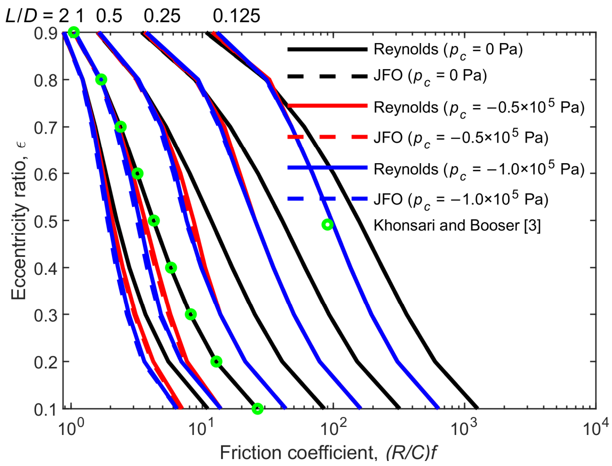

Figure 8. Effect of cavitation pressure on friction coefficient for Reynolds and JFO theory at Λ = 10.

Figure 9 shows the effect of cavitation pressure on the side leakage for the Reynolds model and the JFO theory. The side leakage Q_L is expressed by

$$Q_L = Q_3 + Q_4 \tag{21}$$

The side leakage predicted using the Reynolds model is the same to that predicted using the JFO theory for p_c = 0 Pa (the black dotted lines are covered by the black solid lines), and they agree well with the results provided by Khonsari and Booser [3]. The side leakage decreases with the decreasing cavitation pressure for most cases. This is because the negative gradient means the oil is sucked back into the bearing clearance. In other words, the oil flows away from the positive pressure region and reverses from the negative pressure region. On the other hand, the side leakage remains zero at the low ε and L/D. It is explained by the full Sommerfeld solution: the symmetrical pressure distribution results in an equal outflow and reflux. In addition, the side leakage is overestimated by the Reynolds model, because the pressure gradient in the divergence region is weakened by the underestimated cavitated area, causing the reduction in the inverse flow.

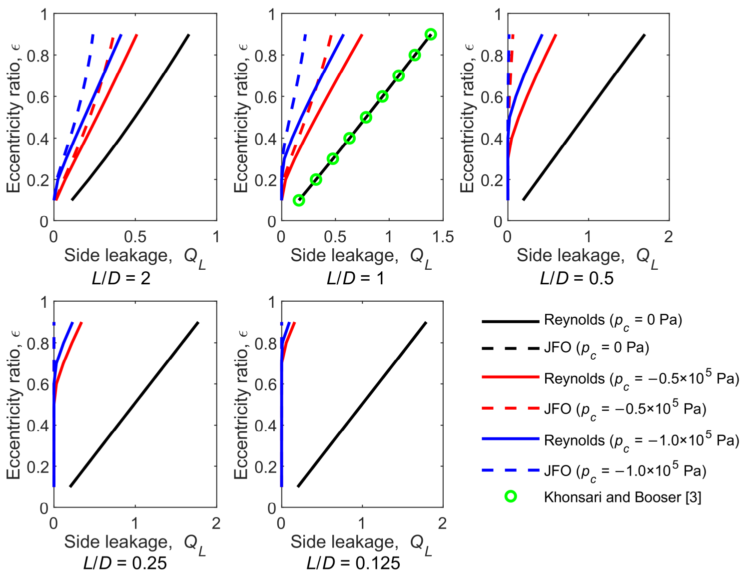

Figure 9. Effect of cavitation pressure on side leakage for Reynolds model and JFO theory at Λ = 10.

Figure 10 shows the effect of cavitation pressure on the net leakage for the Reynolds model and the JFO theory. The net leakage Q_{net} is calculated by

$$Q_{net} = Q_1 - Q_2 - Q_3 - Q_4 \tag{22}$$

The net leakage represents whether the oil film is mass-conserving or not. (1) All the net leakages predicted using the JFO theory are zero, except the case of the cavitation pressure being 0 Pa (the black dotted lines are covered by the black solid lines). In the case, the oil film pressure distribution predicted using the JFO theory is the same to that predicted using the Reynolds model. Hence, the net leakages of the two methods are equal. (2) The absolute net leakage predicted using the Reynolds model increases with the increase in ε and L/D. That is, the non-mass-conserving phenomenon is amplified as the hydrodynamic effect enhances.

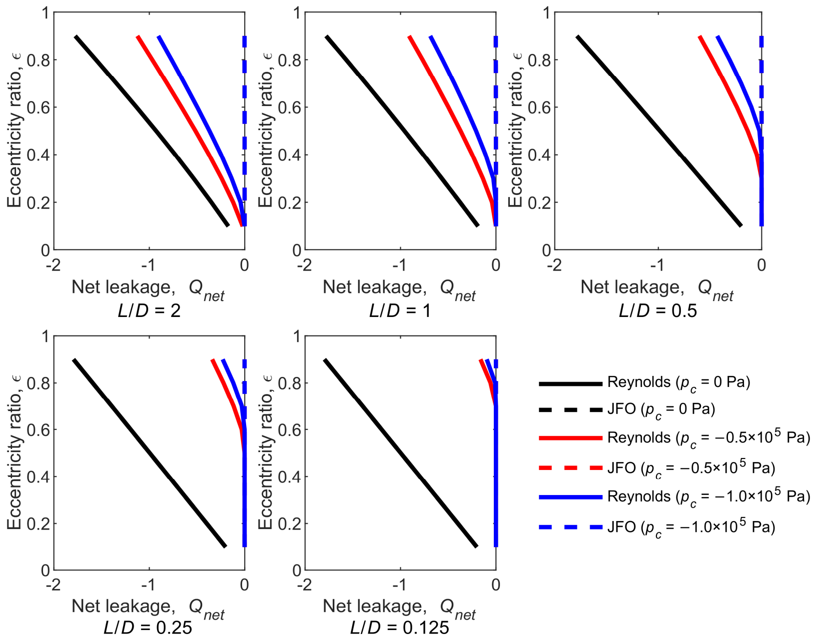

Figure 10. Effect of cavitation pressure on net leakage for Reynolds model and JFO theory at $\Lambda = 10$.

The above analysis is based on the constant bearing number $\Lambda = 10$. The following part shows the effect of the bearing number on the bearing characteristics. Figure 11 shows the effect of the bearing number on the Sommerfeld number for the Reynolds model and the JFO theory. The difference in the Sommerfeld number between different cavitation pressures decreases with the increasing L/D, ε and Λ. In extreme cases, the Sommerfeld number predicted using the Reynolds model is the same to that predicted using the JFO theory at the large L/D, ε and Λ. This is due to the fact that, as the bearing number increases, the hydrodynamic effect enhances, and the cavitation effect is weakened.

The bearing number, as a function of rotational speed, viscosity, and clearance, represents the extent of hydrodynamic effect. Hence, the cavitation effect is weakened with the increased bearing number. The effect of the bearing number on the Sommerfeld number is similar to that on the attitude angle, friction coefficient, and side leakage. Due to the similarity, the corresponding analysis is ignored. These results are provided in Appendix A.

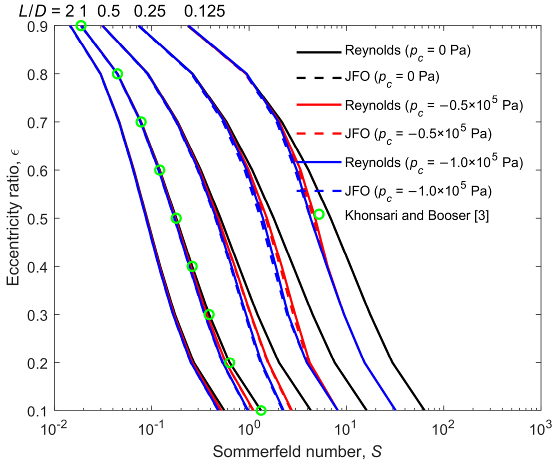

(**a**)

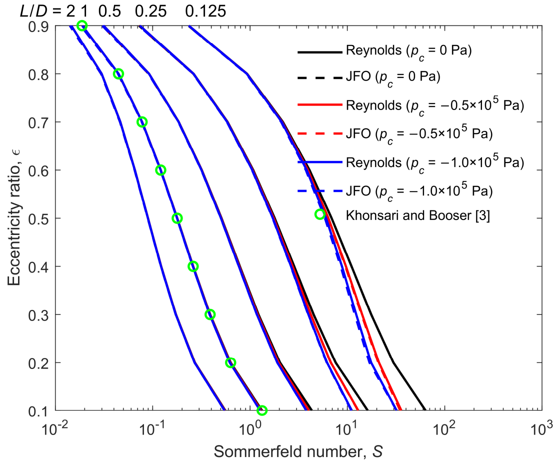

(**b**)

Figure 11. Effect of bearing number on Sommerfeld number for Reynolds model and JFO theory: (**a**) Λ = 100; (**b**) Λ = 1000.

The bearing number, as a function of rotational speed, viscosity, and clearance, represents the extent of hydrodynamic effect. Hence, the cavitation effect is weakened with the increased bearing number. The effect of the bearing number on the Sommerfeld number is similar to that on the attitude angle, friction coefficient, and side leakage. Due to the similarity, the corresponding analysis is ignored. These results are provided in Appendix A.

5. Conclusions

(1) The low cavitation pressure leads to a decrease in the Sommerfeld number, friction coefficient, and side leakage, and an increase in the attitude angle. The cavitation effect is weakened with the increased L/D, eccentricity ratio, and bearing number due to the improvement of the hydrodynamic effect.
(2) The cavitated area is underestimated by the Reynolds model due to the inaccurate oil film reformation boundary, leading to the underestimation of the load-carrying capacity and the overestimation of the friction coefficient and side leakage.
(3) To sum up, the load-carrying capacity is improved by the decrease in the cavitation pressure, and the effect is significant in lightly loaded cavitated bearings. In the non-cavitated case and the cavitated case with intermediate and heavy loads, the difference between the Reynolds model and the JFO theory can be effectively ignored, but the accuracy of the leakage predicted using the Reynolds model should be carefully evaluated.

Author Contributions: Conceptualization, W.X.; investigation, S.Z. and Y.X.; software, K.L.; writing—original draft preparation, W.X.; writing—review and editing, W.X. All authors have read and agreed to the published version of the manuscript.

Funding: This research was funded by the project YKJ201814 supported by Science Foundation of Nanjing Institute of Technology.

Institutional Review Board Statement: Not applicable.

Informed Consent Statement: Not applicable.

Data Availability Statement: Data are contained within the article.

Acknowledgments: The authors are grateful for the project YKJ201814 supported by Science Foundation of Nanjing Institute of Technology.

Conflicts of Interest: The authors declare no conflict of interest.

Appendix A

The effects of attitude angle, friction coefficient, and side leakage for different bearing numbers are shown in Figures A1–A3, respectively.

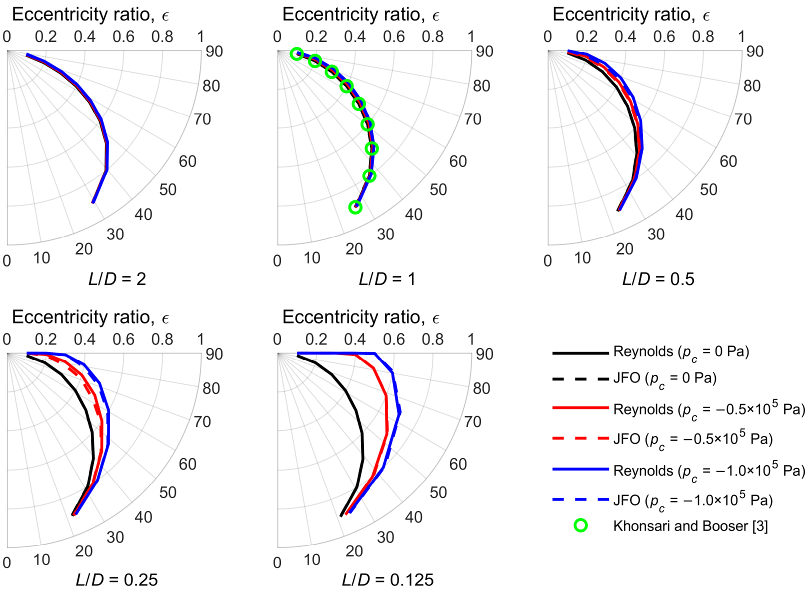

(**a**)

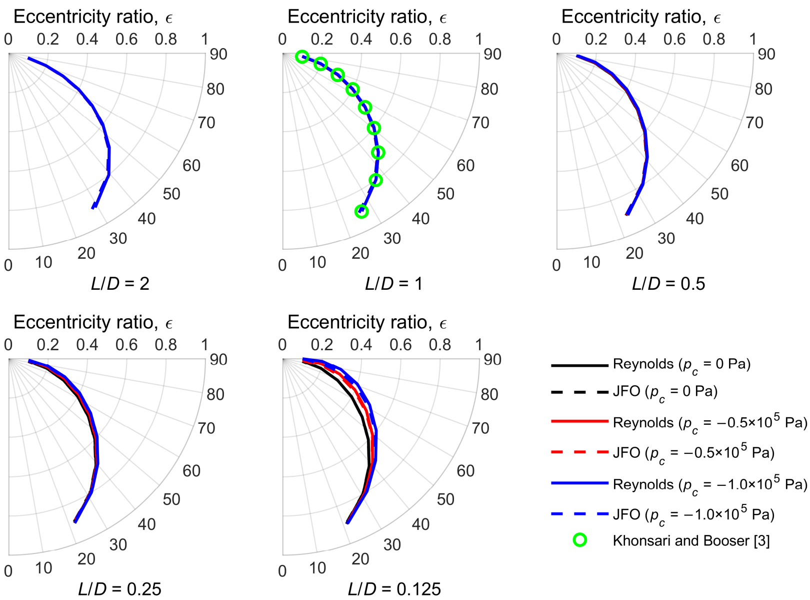

(**b**)

Figure A1. Effect of bearing number on attitude angle for Reynolds model and JFO theory: (**a**) $\Lambda = 100$; (**b**) $\Lambda = 1000$.

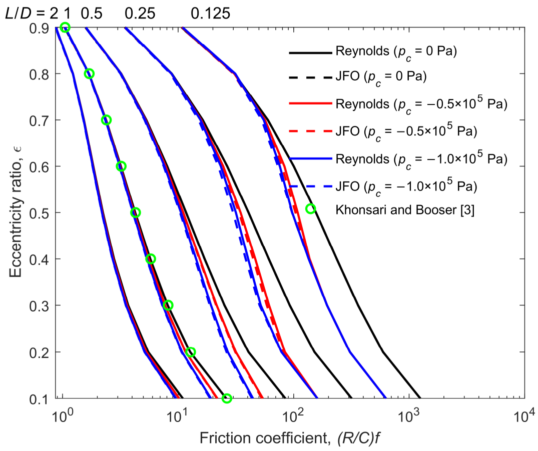

(**a**)

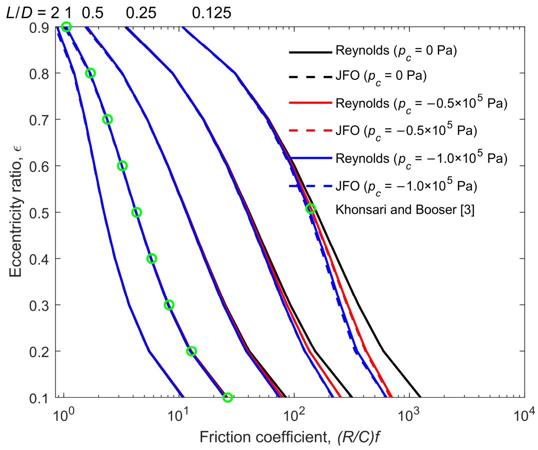

(**b**)

Figure A2. Effect of bearing number on friction coefficient for Reynolds model and JFO theory: (**a**) Λ = 100; (**b**) Λ = 1000.

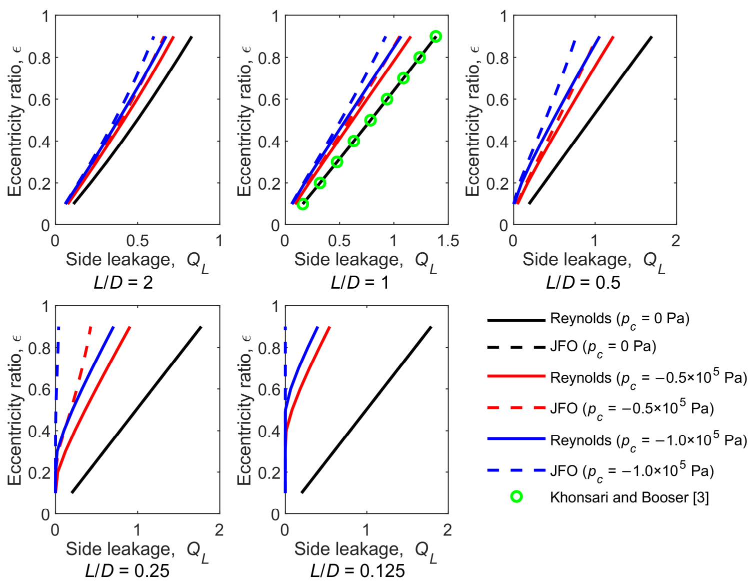

(**a**)

Figure A3. *Cont.*

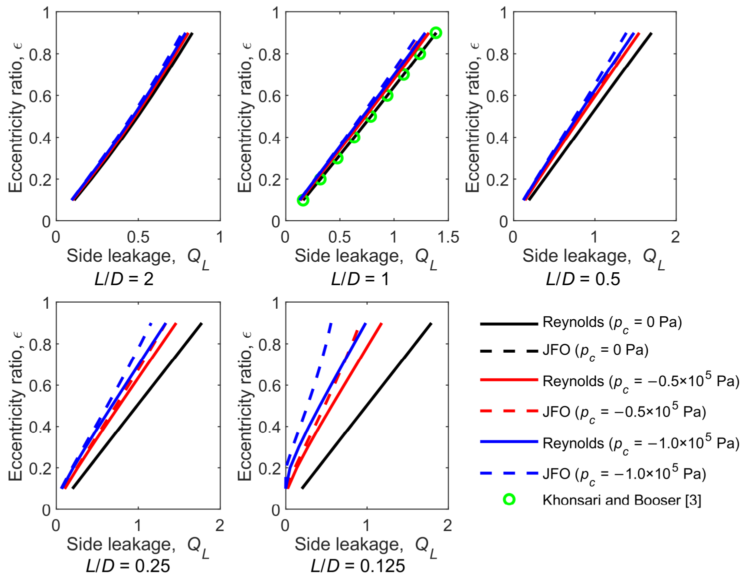

(**b**)

Figure A3. Effect of bearing number on side leakage for Reynolds model and JFO theory: (**a**) Λ = 100; (**b**) Λ = 1000.

References

1. Gropper, D.; Wang, L.; Harvey, T.J. Hydrodynamic Lubrication of Textured Surfaces: A Review of Modeling Techniques and Key Findings. *Tribol. Int.* **2016**, *94*, 509–529. [CrossRef]
2. Braun, M.J.; Hannon, W.M. Cavitation formation and modelling for fluid film bearings: A review. *Proc. Inst. Mech. Eng. Part J J. Eng. Tribol.* **2010**, *224*, 839–863. [CrossRef]
3. Khonsari, M.M.; Booser, E.R. *Applied Tribology: Bearing Design and Lubrication*; John Wiley & Sons: Hoboken, NJ, USA, 2017.
4. Shen, C.; Khonsari, M.M. On the Magnitude of Cavitation Pressure of Steady-State Lubrication. *Tribol. Lett.* **2013**, *51*, 153–160. [CrossRef]
5. Reynolds, O. On the Theory of Lubrication and Its Application to Mr. Beauchamp Tower's Experiments, Including an Experimental Determination of the Viscosity of Olive Oil. *Philos. Trans. R. Soc. Lond.* **1886**, *177*, 157–234.
6. Jakobsson, B.; Floberg, L. The Finite Journal Bearing, Considering Vaporization. *Trans. Chalmers Univ. Technol.* **1957**, *190*.
7. Olsson, K. Cavitation in Dynamically Loaded Bearings. *Trans. Chalmers Univ. Technol.* **1965**, *308*.
8. Christopherson, D.G. A New Mathematical Method for the Solution of Film Lubrication Problems. *Proc. Inst. Mech. Eng.* **1941**, *146*, 126–135. [CrossRef]
9. Xu, W.; Tian, Y.; Song, Y.; Zhang, M.; Yang, J. Reynolds Boundary Condition Approximation in Journal Bearings Based on Dynamic Mesh Method. *Tribol. Online* **2021**, *16*, 81–88. [CrossRef]
10. Ausas, R.; Ragot, P.; Leiva, J.; Jai, M.; Bayada, G.; Buscaglia, G.C. The Impact of the Cavitation Model in the Analysis of Microtextured Lubricated Journal Bearings. *J. Tribol.* **2007**, *129*, 868–875. [CrossRef]
11. Qiu, Y.; Khonsari, M.M. On the Prediction of Cavitation in Dimples Using a Mass-Conservative Algorithm. *ASME J. Tribol.* **2009**, *131*. [CrossRef]
12. Muchammad, M.; Tauviqirrahman, M.; Jamari, J.; Schipper, D.J. Analysis of the Effect of the Slip-Pocket in Single and Double Parallel Bearing Considering Cavitation: A Theoretical Approach. *Lubricants* **2021**, *9*, 3. [CrossRef]
13. Elrod, H.G. A Cavitation Algorithm. *J. Lubr. Technol.* **1981**, *103*, 350–354. [CrossRef]
14. Vijayaraghavan, D.; Keith, T.G. Development and Evaluation of a Cavitation Algorithm. *Tribol. Trans.* **1989**, *32*, 225–233. [CrossRef]
15. Giacopini, M.; Fowell, M.T.; Dini, D.; Strozzi, A. A Mass-Conserving Complementarity Formulation to Study Lubricant Films in the Presence of Cavitation. *J. Tribol.* **2010**, *132*, 041702. [CrossRef]
16. Almqvist, A.; Fabricius, J.; Larsson, R.; Wall, P. A New Approach for Studying Cavitation in Lubrication. *J. Tribol.* **2013**, *136*, 011706. [CrossRef]
17. Xu, W.; Li, K.; Geng, Z.; Zhang, M.; Yang, J. A Local Adaptive Mesh Refinement for JFO Cavitation Model on Cartesian Meshes. *Appl. Sci.* **2021**, *11*, 9879. [CrossRef]
18. Pap, B.; Fillon, M.; Guillemont, M.; Bauduin, L.; Chocron, J.; Gédin, P.; Biadalla, L. Experimental and Numerical Analysis on the Seizure of a Carbon-Filled PTFE Central Groove Journal Bearing during Start-Up Period. *Lubricants* **2018**, *6*, 14. [CrossRef]

19. Nogi, T.; Soma, M.; Dong, D. Numerical Analysis of Grease Film Thickness and Thickener Concentration in Elastohydrodynamic Lubrication of Point Contacts. *Tribol. Trans.* **2020**, *63*, 924–934. [CrossRef]
20. Dowson, D.; Taylor, C.M. Cavitation in Bearings. *Annu. Rev. Fluid Mech.* **1979**, *11*, 35–65. [CrossRef]
21. Rasep, Z.; Muhammad Yazid, M.N.A.W.; Samion, S. Lubrication of textured journal bearing by using vegetable oil: A review of approaches, challenges, and opportunities. *Renew. Sustain. Energy Rev.* **2021**, *146*, 111191. [CrossRef]
22. Brizmer, V.; Kligerman, Y. A Laser Surface Textured Journal Bearing. *J. Tribol.* **2012**, *134*. [CrossRef]
23. Kango, S.; Sharma, R.; Pandey, R.K.J.T.I. Thermal analysis of microtextured journal bearing using non-Newtonian rheology of lubricant and JFO boundary conditions. *Tribol. Int.* **2014**, *69*, 19–29. [CrossRef]
24. Lu, X.; Khonsari, M.M. An Experimental Investigation of Dimple Effect on the Stribeck Curve of Journal Bearings. *Tribol. Lett.* **2007**, *27*, 169. [CrossRef]
25. Xie, Z.; Zhu, W. An investigation on the lubrication characteristics of floating ring bearing with consideration of multi-coupling factors. *Mech. Syst. Signal Process.* **2022**, *162*, 108086. [CrossRef]
26. Xie, Z.; Zhu, W. Theoretical and experimental exploration on the micro asperity contact load ratios and lubrication regimes transition for water-lubricated stern tube bearing. *Tribol. Int.* **2021**, *164*, 107105. [CrossRef]
27. Manser, B.; Belaidi, I.; Hamrani, A.; Khelladi, S.; Bakir, F. Texture shape effects on hydrodynamic journal bearing performances using mass-conserving numerical approach. *Tribol.-Mater. Surf. Interfaces* **2020**, *14*, 33–50. [CrossRef]
28. Han, Y.; Fu, Y. Comparison of hydrodynamic characteristics between circumferential and transversal microgrooved journal bearings. *Lubr. Sci.* **2019**, *31*, 285–298. [CrossRef]
29. Sharma, N.; Verma, R.; Sharma, S.; Kango, S. Qualitative potentials of surface textures and coatings in the performance of fluid-film bearings: A critical review. *Surf. Topogr. Metrol. Prop.* **2021**, *9*, 013002. [CrossRef]
30. Galda, L.; Sep, J.; Olszewski, A.; Zochowski, T. Experimental investigation into surface texture effect on journal bearings performance. *Tribol. Int.* **2019**, *136*, 372–384. [CrossRef]
31. Yamada, H.; Taura, H.; Kaneko, S. Numerical and Experimental Analyses of the Dynamic Characteristics of Journal Bearings With Square Dimples. *J. Tribol.* **2017**, *140*, 011703. [CrossRef]
32. Shinde, A.; Pawar, P.; Shaikh, P.; Wangikar, S.; Salunkhe, S.; Dhamgaye, V. Experimental and Numerical Analysis of Conical Shape Hydrodynamic Journal Bearing With Partial Texturing. *Procedia Manuf.* **2018**, *20*, 300–310. [CrossRef]
33. Fesanghary, M.; Khonsari, M.M. A Modification of the Switch Function in the Elrod Cavitation Algorithm. *J. Tribol.* **2011**, *133*, 024501. [CrossRef]
34. Cupillard, S.; Glavatskih, S.; Cervantes, M.J. Computational Fluid Dynamics Analysis of a Journal Bearing with Surface Texturing. *Proc. Inst. Mech. Eng. Part J J. Eng. Tribol.* **2008**, *222*, 97–107. [CrossRef]
35. Brewe, D.E. Theoretical Modeling of the Vapor Cavitation in Dynamically Loaded Journal Bearings. *J. Tribol.* **1986**, *108*, 628–637. [CrossRef]
36. Hamrock, B.J.; Schmid, B.J.; Jacobson, B.O. *Fundamentals of Fluid Film Lubrication*; CRC Press: Boca Raton, FL, USA, 2004; Volume 169.
37. Stachowiak, G.; Batchelor, A.W. *Engineering Tribology*; Butterworth-Heinemann: Oxford, UK, 2013.